Solid-State Structures

Deutsche Ausgabe: DOI: 10.1002/ange.201602066
Internationale Ausgabe: DOI: 10.1002/anie.201602066

$HfMnSb_2$: A Metal-Ordered NiAs-type Pnictide with a Conical Spin Order

*Taito Murakami, Takafumi Yamamoto, Cédric Tassel, Hiroshi Takatsu, Clemens Ritter, Yoshitami Ajiro, and Hiroshi Kageyama**

Abstract: *The NiAs-type structure is one of the most common structures in solids, but metal order has been almost exclusively limited to chalcogenides. The synthesis of $HfMnSb_2$ is reported with a novel metal-ordered NiAs-type structure. $HfMnSb_2$ undergoes a conical spin order below 270 K, in marked contrast to conventional magnetic order observed in NiAs-type pnictides. We argue that the layered arrangement of Hf and Mn makes it a quasi 2D magnet, where the Mn layers with localized magnetic moments (Mn^{2+}; $S = 5/2$) can interact only through RKKY interactions, instead of metal–metal bonding that is otherwise dominant for typical NiAs-type pnictides. This result suggests that controlling order–disorder in NiAs-type pnictides enables a study of 2D-to-3D crossover behavior in itinerant magnetic system.*

The rock-salt (NaCl) and nickel arsenide (NiAs) structures are by far the most common structures to be found in solid-state chemistry, where anions X are arranged in cubic and in hexagonal close packing, with all the interstitial octahedral voids occupied by the cations A. As for the latter, each AX_6 octahedron is edge-shared with six octahedra in the hexagonal plane while face-shared with two octahedra along *c*. The face-sharing structure is stabilized by direct metal–metal orbital overlap. Thus, NiAs-type compounds are generally metallic.[1]

Cation order in the NaCl-type oxides not only enriches the structural chemistry but also provides new or improved properties. The most commonly encountered is a 1:1 order.[2] Most of them are isostructural with β-$LiFeO_2$, γ-$LiFeO_2$, or α-$NaFeO_2$ having different cation-ordered patterns. These materials have been intensively studied, for example, as cathode materials for secondary batteries and catalysts for oxidative coupling of methane.[3] Compounds with 2:1 and 5:1 order are also known.[2] The NiAs-type structure is also capable of forming cation order, but only with the 1:1 order in a layered arrangement known as a $LiTiS_2$-type structure. Many examples are found in chalcogenides $A^+B^{3+}Ch_2$ (Ch = S, Se, Te).[4–10] Particularly interesting is the case when B^{3+} is a magnetic ion, as the layered cation order introduces geometrical frustration based on a triangular lattice, combined with itinerancy. For example, $LiVS_2$ shows an anomalous metallic state.[11]

Many pnictides adopt the NiAs-type structure. They show itinerant ferromagnetism (MnSb, MnBi) and antiferromagnetism (CrSb, $Fe_{1+x}Sb$) and superconductivity (NiBi).[1] However, cation order has not been reported. Herein, we report a new NiAs-type antimonide $HfMnSb_2$ with a cation order. We found that $HfMnSb_2$ is a quasi-two-dimensional (2D) itinerant magnet with a conical spin structure. The origins of metal order and spin structure are discussed.

$HfMnSb_2$ was synthesized by solid-state reaction using Hf, Mn, and Sb. When the stoichiometric mixture was reacted at 800 °C for 48 h, the X-ray diffraction (XRD) profile mainly showed $HfSb_2$ and MnSb (Supporting Information, Figure S1). However, an off-stoichiometric condition led to a new hexagonal phase, along with HfSb. The least HfSb was achieved for Hf:Mn:Sb = 1:1:1.8. Energy-dispersive X-ray spectroscopy (EDX) gave the molar ratio of the new phase to be Hf:Mn:Sb = 25.3:25.5:49.3 (Supporting Information, Figure S2), in agreement with $HfMnSb_2$. Evaporated powder on the glass surface has a ratio of Hf:Mn = 54.7:45.3, which accounts for the Sb-deficient condition employed.

The XRD pattern resembles with those of NiAs-type MnSb ($P6_3/mmc$).[1] However, the absence of extinctions (for example, 00*l*) strongly suggests metal order into a layered arrangement, in which the original Ni site splits into 1*a* and 1*b* for $P3{-}m1$, one of the subgroups of $P6_3/mmc$. Accordingly, Rietveld refinement of the synchrotron XRD (SXRD) profile (Figure 1 a) was performed using the $LiTiS_2$-type structure. HfSb impurity (1.95 wt %) was included as a secondary phase. The refinement converged successfully (Table 1). No cation

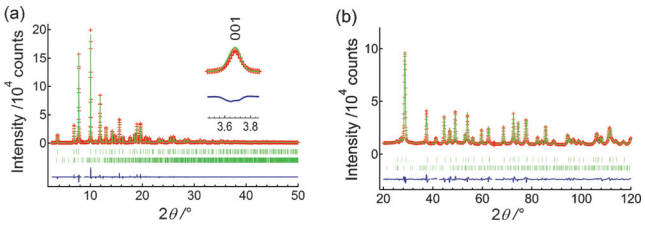

Figure 1. a) SXRD and b) ND patterns of $HfMnSb_2$. Red crosses and green and blue lines represent observed, calculated, and difference profiles. Upper/lower ticks represent the positions of Bragg peaks of $HfMnSb_2$ and HfSb. There are several unindexed peaks (not assigned as any superreflections) which were excluded from the refinement.

[*] T. Murakami, Dr. T. Yamamoto, Dr. C. Tassel, Dr. H. Takatsu, Prof. Y. Ajiro, Prof. H. Kageyama
Graduate School of Engineering, Kyoto University
Kyoto 615-8510 (Japan)
E-mail: kage@scl.kyoto-u.ac.jp
Dr. C. Ritter
Institut Laue-Langevin
6, rue Jules Horowitz, Grenoble 38000 (France)
Supporting information and the ORCID identification number(s) for the author(s) of this article can be found under: http://dx.doi.org/10.1002/anie.201602066.

Table 1: Structural parameters of $HfMnSb_2$ from SXRD (ND) data.[a]

Atom	Site	*g*	*x*	*y*	*z*	U_{iso}/100 Å^2
Hf1	1*b*	0.944(2) (0.918(4))	0	0	1/2	0.13(2) (1.38(7))
Mn1	1*a*	0.056(2) (0.082(4))	0	0	0	0.13(2) (1.38(7))
Mn2	1*a*	0.944(2) (0.918(4))	0	0	0	0.21(2) (2.23(17))
Hf2	1*b*	0.056(2) (0.082(4))	0	0	1/2	0.21(2) (2.23(17))
Sb	2*d*	1	1/3	2/3	0.2377(2) (0.2395(2))	0.346(15) (1.09(5))

[a] *P*3−*m*1, $a = 4.0594(4)$ (4.0546(11)) Å, $c = 6.5512(6)$ (6.5372(2)) Å, $R_{wp} = 7.94\%$ (3.98%), $R_p = 5.39\%$ (2.89%), GOF = 3.60 (4.51).

and anion deficiency was detected. Inspection of cation disorder revealed a small degree of anti-site disorder (5.6%).

Almost the same result was obtained from the analysis of neutron diffraction (ND) data (Figure 1b). Thus, we conclude $HfMnSb_2$ crystallizes in the $LiTiS_2$-type structure (Figure 2).

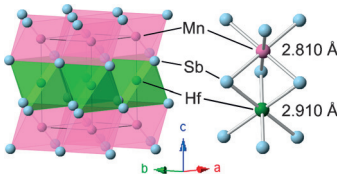

Figure 2. Left: Structure of $HfMnSb_2$ with the $LiTiS_2$-type structure. Note that a small degree of *anti*-site cation disorder (5.6%) is present. Right: Coordination geometry around Mn and Hf.

The *z* coordinate of 0.238 for Sb (away from $z = 1/4$) means the alternation of Sb–Sb distance along *c*, providing a justification of the metal order. The resultant Hf–Sb distance of 2.910 Å is comparable to those of binary hafnium antimonides (2.804–3.175 Å).[12] A shorter distance is found in Mn–Sb bonding (2.810 Å), which is within the range of 2.798–2.887 Å in binary manganese antimonides.[1,13]

The $LiTiS_2$-type structure has been almost exclusively limited to chalcogenides ($A^+B^{3+}Ch_2$).[9–11] These are prepared either by solid-state syntheses (such as $TlCrTe_2$, $CdInS_2$),[4–6,14] or by intercalation reactions for CdI_2-type compounds (such as $LiVS_2$, $KCrSe_2$).[7–10] Metal-deficient phases are also observed (for example, $Fe_{0.16}ZrSe_{1.94}$, $Cr_{0.25}TiTe_2$, $Ti_{0.33}TiTe_2$[15]). Other than chalcogenides, only two stannides, $AuNiSn_2$ and $AuCuSn_2$, adopt this structure.[16] Regarding pnictides, there exist only disordered NiAs-type compounds such as $Mn_{1-x}Ti_xSb$.[17,18] Among a vast number of pnictides with $ABPn_2$ (Pn = P, As, Sb, Bi), a 1:1 metal-order is achieved in the $SrZnBi_2$-type (for example, $BaMnSb_2$), $HfCuSi_2$-type (for example, $LaAgSb_2$), and $SrZnSb_2$,[19–23] all of which contain alternately stacked BPn and Pn layers intervened by A (Supporting Information, Figure S3).

Apart from intercalated products, the origin of cation order in NiAs-type $ABCh_2$ has not been explicitly addressed, but highly polarizable chalcogen anions likely allow cation order in a layered fashion. Namely, chalcogen anions in $ABCh_2$ have a tendency to be polarized toward the higher charged B^{3+}. The ionic model is often used in Zintl-related phases in attempting to formulate to a first approximation of an oxidation-state assignment. Although the Sb electronegativity is not high, when this model is applied to $HfMnSb_2$, the metal ordering may be understood by the high polarizability of Sb, combined with the charge difference (Hf^{4+} vs. Mn^{2+}). Additionally, the layered metal ordering allows Hf–Sb and Mn–Sb bonds to find optimal distances, as mentioned above. This can avoid electrostatic repulsions between Hf^{4+} ions in face-shared octahedra. It is worth noting, however, that cation order is absent in $(Ti_{0.5}Mn_{0.5})Sb$,[18] which might be explained by a small difference of electronegativity between Ti and Mn. We can also rationalize metal order in $HfMnSb_2$ based on a covalent picture. Here, a pronounced difference in covalent radii (Hf: 1.52 Å, Mn: 1.19 Å) is possibly a key, as discussed for stannides.[24] The absence of metal order in $(Ti_{0.5}Mn_{0.5})Sb$ is also understood by a closer covalent radius of Ti (1.36 Å) to Mn.

First-principle calculations were performed, assuming a ferromagnetic structure for simplicity. The density of states (DOS) near the Fermi energy E_F (Figure 3) shows

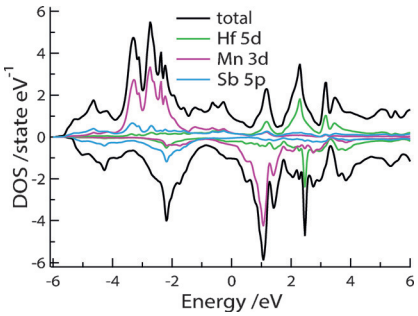

Figure 3. The computed DOS of $HfMnSb_2$. Positive (negative) values represent spin majority (minority) components.

that the Mn 3d orbital is fairly localized and largely polarized by a large exchange splitting between the spin majority and minority components. The Mn valence estimated from the contribution of Mn 3d orbital below E_F yielded $Mn^{1.9+}$ ($d^{5.1}$), consistent with the high-spin-state Mn^{2+}. On the contrary, the Hf 5d orbital is rather dispersive and only weakly polarized, and a smaller Hf valence of +2.7 is obtained (inconsistent with the ionic model). The discrepancy from the ionic picture is reasonable given a relatively small electronegativity of Sb. A finite DOS at E_F implies a metallic conductivity, which is indeed experimentally observed in the temperature dependence of the resistivity (Figure 4d).

The temperature variation of magnetization (Figure 4a) exhibits a rapid increase at around 260–290 K, implying a transition to a ferromagnetic (FM) state. From the Arrott plot (Figure 4b), we obtained T_C of 270 K, which is lower than those of NiAs-type MnPn (for example, 587 K for Sb, 628 K for Bi),[1] reflecting the 2D structure of $HfMnSb_2$.

The *M*–*H* curve at 5 K (Figure 4c) shows a saturating behavior with a moment of 2.95 μ_B/Mn at 7 T (remnant moment of 0.71 μ_B and coercive field of 43 Oe). The saturation moment is comparable with 3.6 μ_B obtained from

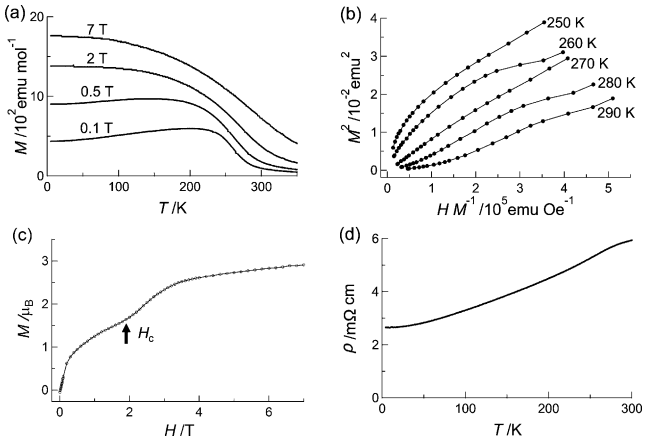

Figure 4. a) M vs. T at various fields. b) Arrott plot. c) M–H curve at 5 K. d) Resistivity ρ vs. T.

the calculations and with those in MnPn.[1] However, unlike MnPn with a typical hysteresis loop, $HfMnSb_2$ has a plateau-like slope below $H_c \approx 2$ T, suggesting the ground state to be ferrimagnetic (FRM). To obtain evidence for the FRM state, NPD data were collected at low temperatures (Supporting Information, Figure S4). The profiles around 001 and 101 (Figure 5c) show satellite peaks with an incommensurate k-vector (0, 0, 0.14) the intensities of which decrease with T and vanish above T_C, confirming a magnetic origin of this transition.

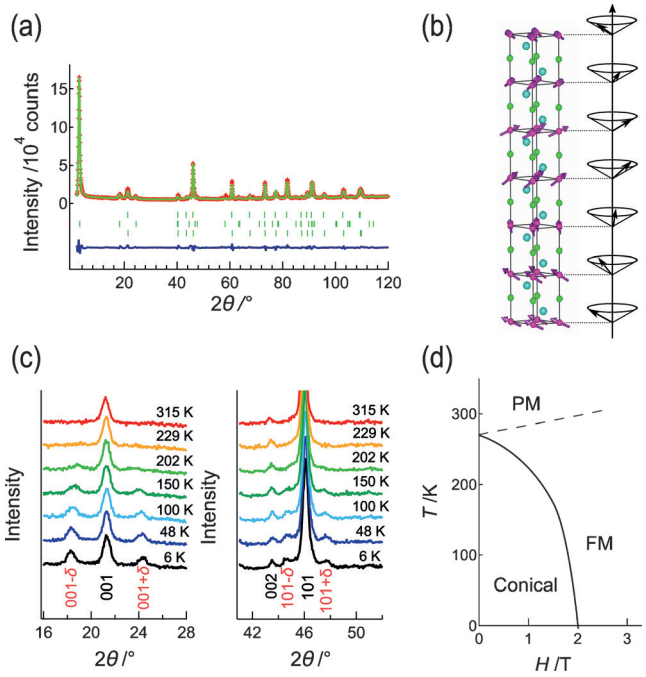

Figure 5. a) Magnetic Rietveld refinement of ND for $HfMnSb_2$ at 6 K. Red crosses and green and blue lines represent observed, calculated, and difference intensities. Upper, middle, and lower ticks represent the positions of Bragg peaks of nuclear, AFM, and FM components. b) Conical structure at 6 K. The Mn moment is tilted by 15° away from the *ab* plane. c) Incommensurate peaks near 001 and 101. d) Phase diagram as a function of T and H, where PM stands for a paramagnetic state.

The FM component below T_C evidenced by the Arrott plot and the AFM component evidenced by NPD indicate a conical structure as shown in Figure 5b. Refinement of the 6 K data (Figure 5a) gave 2.627(28) μ_B and 0.688(236) μ_B, respectively, for AFM and FM components ($R_{wp} = 17.6\,\%$, GOF = 7.13). This provides a total moment of 2.76(7) μ_B, in agreement with 2.95 μ_B from the M–H curve. The small H_c implies that the conical phase is located in the vicinity of the phase boundary to FM phase. The T–H phase diagram is given in Figure 5d.

It is naturally conceived that the in-plane Mn−Mn interaction is FM, as verified by the Mn-Sb-Mn angle of 92.5° according to the Goodenough–Kanamori rules, a situation often found in NiAs-type compounds.[1] However, the incommensurate k-vector along c is distinct from commensurate ones in MnPn and CrSb. In NiAs-type pnictides, the metal–metal distance of the face-sharing octahedra is within the range of direct metal–metal bonding and makes their magnetism fairly 3D. In contrast, the Mn moments in $HfMnSb_2$ are well-separated along c (6.55 Å) by nonmagnetic Hf. It means that the out-of-plane interaction in $HfMnSb_2$ is essentially different in origin from NiAs-type pnictides (direct metal–metal bonding).

These considerations led us to search for other layered systems with a conical spin order. We noticed that MMn_2Ge_2 with Mn_2Ge_2 sheets separated by M (M = La, Ce, Pr, and Nd) has such a spin structure,[25] though the Mn layer has a square lattice, not a triangular one. For MMn_2Ge_2, it was argued that long-range RKKY (Ruderman–Kittel–Kasuya–Yosida) interactions via mobile electrons are a primary source of the out-of-plane Mn−Mn coupling, giving frustrated interactions and hence the conical spin order.[26] The closeness of Mn−Mn distance between $HfMnSb_2$ and MMn_2Ge_2 suggests the RKKY-derived mechanism could be applicable to $HfMnSb_2$.

In conclusion, we prepared $HfMnSb_2$ as the first example of a metal-ordered NiAs structure among pnictides. It shows a conical spin order, arising from dimensional reduction. Layered pnictides have been intensively studied because of various properties like high-T_c superconductivity.[27] However, our system provides a new direction in the study of itinerant magnetism. For example, $Ti_{0.5}Mn_{0.5}Sb$ with disordered NiAs structure is a FM metal with $T_C \approx 350$ K,[17] reflecting the 3D structure. The possession of ordered- and disordered-NiAs structures allows a new opportunity to systematically tune direct exchange and RKKY interactions and observe 2D-to-3D crossover by $(Hf_{1-x}Ti_x)MnSb_2$, which is now in progress. Controlling the degree of *anti*-site disorder in $HfMnSb_2$ by tuning synthetic conditions is an alternative approach. It is also expected that other $LiTiS_2$-type antimonides with novel physical properties will also be explored.

Acknowledgements

This work was supported by Grant-in-Aid for Scientific Research (A) (No. 16H02267), Young Scientist Grant B from MEXT and CREST. We thank G. Nilsen for his help in neutron experiments. SXRD experiments were performed at SPring-8 (2014B1104, 2013A1360).

Keywords: cation order · conical spin order · NiAs structure · pnictides · solid-state structures

How to cite: *Angew. Chem. Int. Ed.* **2016**, *55*, 9877–9880
Angew. Chem. **2016**, *128*, 10031–10034

[1] K. Motizuki, H. Ido, T. Itoh, M. Morifuji, *Springer Ser. Mater. Sci.* **2009**, *131*, 1.
[2] G. C. Mather, C. Dussarrat, J. Etourneau, A. R. West, *J. Mater. Chem.* **2000**, *10*, 2219, and references therein.
[3] R. K. Ungar, X. Zhang, R. M. Lambert, *Appl. Catal.* **1988**, *42*, Ll.
[4] H. Boller, K. O. Klepp, K. Kirchmayr, *Mater. Res. Bull.* **1995**, *30*, 365.
[5] L. D. Gulay, J. Stępień-Dammb, M. Daszkiewicz, A. Pietraszko, *J. Alloys Compd.* **2007**, *431*, L1.
[6] V. Y. Shemet, L. D. Gulay, I. D. Olekseyuk, *J. Alloys Compd.* **2006**, *426*, 186.
[7] J. G. White, H. L. Pinch, *Inorg. Chem.* **1970**, *9*, 2581.
[8] B. van Laar, D. J. W. Ijdo, *J. Solid State Chem.* **1971**, *3*, 590.
[9] G. A. Wiegers, R. van der Meer, H. van Heinlugen, H. J. Kloosterboer, A. J. A. Alberink, *Mater. Res. Bull.* **1974**, *9*, 1261.
[10] B. Van Laar, F. M. R. Engelsman, *J. Solid State Chem.* **1973**, *6*, 384.
[11] N. Katayama et al., *Phys. Rev. Lett.* **2009**, *103*, 146405.
[12] a) H. Kleinke, B. Harbrecht, *Z. Anorg. Allg. Chem.* **2000**, *626*, 1851; b) A. Kjekshus, *Acta Chem. Scand.* **1972**, *26*, 1633; c) H. Kleinke, C. Felser, *J. Alloys Compd.* **1999**, *291*, 73; d) S. Rundqvist, Y. Andersson, S. Pramatus, *J. Solid State Chem.* **1979**, *28*, 47.
[13] a) J. Nuss, U. Wedig, M. Jansen, *Z. Kristallogr.* **2006**, *221*, 554; b) T. Yamashita, H. Takizawa, T. Sasaki, K. Uheda, T. Endo, *J. Alloys Compd.* **2003**, *348*, 220.
[14] G. D. Guseinov, G. B. Abdullaev, E. M. Kerimova, *Mater. Res. Bull.* **1969**, *4*, 807.
[15] a) A. Gleizes, J. Revelli, J. A. Ibers, *J. Solid State Chem.* **1976**, *17*, 363; b) Z. Huang, W. Bensch, D. Benea, H. Ebert, *J. Solid State Chem.* **2005**, *178*, 2778; c) T. Matkovic, P. Matkovic, *Metalurgija* **1992**, *31*, 107.
[16] S. Lange, T. Nilges, R.-D. Hoffmann, R. Pöttgen, *Z. Anorg. Allg. Chem.* **2006**, *632*, 1163.
[17] T. Hirone, S. Maeda, I. Tsubokawa, N. Tsuya, *J. Phys. Soc. Jpn.* **1956**, *11*, 1083.
[18] T. Kamimura, H. Ido, M. Sato, T. Suzuki, *J. Magn. Magn. Mater.* ***1986***, *54–57*, *939.*
[19] G. Cordier, H. Schaefer, *Z. Naturforsch. B* **1977**, *32*, 383.
[20] E. Brechtel, G. Cordier, H. Schäfer, *J. Less-Common Met.* **1981**, *79*, 131.
[21] P. Wollesen, W. Jeitschko, M. Brylak, L. Dietrich, *J. Alloys Compd.* **1996**, *245*, L5.
[22] M. Brylak, M. H. Möller, W. Jeitschko, *J. Solid State Chem.* **1995**, *115*, 305.
[23] E. Brechtel, G. Cordier, H. Schafer, *Z. Naturforsch. B* **1979**, *34*, 251.
[24] S. Lange, F. M. Schappacher, D. Johrendt, T. Nilges, R.-D. Hoffmann, R. Pöttgena, *Z. Anorg. Allg. Chem.* **2006**, *632*, 1432.
[25] R. Welter, G. Venturini, E. Ressouche, B. Malaman, *J. Alloys Compd.* **1995**, *218*, 204.
[26] N. P. Kolmakova, A. A. Sidorenko, R. Z. Levitin, *Low Temp. Phys.* **2002**, *28*, 653.
[27] Y. Kamihara, T. Watanabe, M. Hirano, H. Hosono, *J. Am. Chem. Soc.* **2008**, *130*, 3296.

Received: March 2, 2016
Revised: May 8, 2016
Published online: June 29, 2016

